

Towards Estimating the Stiffness of Soft Fruits using a Piezoresistive Tactile Sensor and Neural Network Schemes

Frank Efe Erukainure¹, Victor Parque², Mohsen A. Hassan³ and Ahmed M.R. FathElbab⁴

Abstract—Measuring the ripeness of fruits is one of the key challenges to enable optimal and just-in-time strategies across the fruit supply chain. In this paper, we study the performance of a tactile sensor to estimate the ground truth of the stiffness of fruits, with kiwifruit as a case study. Our sensor configuration is based on a three-beam cantilever arrangement with piezoresistive elements, enabling the stable acquisition of sensor readings over independent trials. Our estimation scheme is based on the compact feed-forward neural networks, allowing us to find effective nonlinear relationships between instantaneous sensor readings and the ground truth of stiffness of fruits. Our experiments using several kiwifruit specimens show the competitive performance frontiers of stiffness approximation using 25 compact feed-forward neural networks, converging to MSE loss at 10^{-5} across training-validation-testing in most of the cases, and the utmost predictive performance of a pyramidal class of feed-forward architectures. Our results pinpoint the potential to realize robust fruit ripeness measurement with intelligent tactile sensors.

I. INTRODUCTION

About one-third of all fresh fruits are lost along the fruit supply chain before they are finally consumed. Postharvest losses occur mainly as a result of rough handling, poor packaging, lack of temperature management, and lack of public awareness on the need to maintain quality [1]. Meanwhile, fruits are harvested when mature and hard to avoid postharvest losses. The harvested fruits are usually stored and, as a result, ripen more and lose their stiffness over a short period. However, a change in color doesn't guarantee the ripeness of most fruits; ripeness is often times estimated by touching the fruit and applying little force with one's fingers. This method will lead to a further deterioration of the fruit's quality (such as taste and appearance) and hence a change in its mechanical properties (such as stiffness or hardness).

Kiwifruit is a soft nutritious fruit which suffers mechanical compression damage easily in many ways, such as during picking, packaging, transporting, and marketing [2]. Due to the appearance of kiwifruit, it is often difficult to determine its ripeness and mechanical properties without having to touch its

surface and apply some form of pressure. Hence, the market quality of the fruit is negatively affected, as earlier mentioned. This has become an issue of concern to farmers and marketers of fruits. The availability of effective ripeness detection devices, such as tactile sensors, is potential in tackling these challenges.

The recognition of carrot appearance quality using deep learning techniques was studied by [3] and [4], where they proposed a ResNet101 plus Support Vector Machine (SVM), and an improved dense capsule network model (Modified-DCNet) respectively. Their techniques, however, had limitations as there were some misclassifications due to the fact that the carrot surface contained many bent and defected areas and as a result, many shadows were generated across the carrot surface (i.e., due to uneven illumination). The use of tactile sensors to extract the mechanical features of fruits before training the extracted features with a suitable machine learning (ML) algorithm is potential to solve the challenges of misclassifications. Other studies for fruit and plant features identification based on computer vision and image processing were conducted by [5]–[7], but these studies are mostly limited to image recognition techniques and cannot be effectively employed in detecting the internal mechanical features of fruits such as stiffness and elastic modulus.

Tactile sensors for contact force estimation have been developed, and several prototypes have been proposed as in [8], [9]. However, these sensors have focused more on force sensing and pressure sensing; just few studies have been conducted on elasticity sensing, which focuses on the stiffness factor. In [10], the firmness of kiwifruit was effectively determined by a combination of acoustic vibration sensor and CARS algorithm, and it was observed that a combination of sensor signals with machine learning algorithm could well characterize the firmness of kiwifruit. Other approaches for stiffness characterization using machine learning algorithms were studied in [11]–[13]. A similar approach will be utilized in this paper for accurate measurement of the stiffness of fruits via a combination of extracted features of our proposed tactile sensor and a ML algorithm to classify the features and make accurate estimation of the stiffness of fruits.

On the other hand, some of the concepts applied in tactile sensing of soft tissue stiffness properties have been published by [14]–[16]. In [14], [15], a two-tip tactile sensing technique was developed; but the disadvantage of the two-tip model is that the sensor's output is unstable during experiments due to surface irregularity and large inclination angle of soft tissue surfaces. In [16], the output of the proposed sensor configu-

*This work was supported by the generous contribution of Japan International Cooperation Agency (JICA)

¹Frank Efe Erukainure is with the Department of Mechatronics and Robotics Engineering, Egypt-Japan University of Science and Technology, Alexandria, Egypt frank.erukainure@ejust.edu.eg

²Victor Parque is with the Department of Modern Mechanical Engineering, Waseda University, Tokyo, Japan parque@aoni.waseda.jp

³Mohsen A. Hassan is with the Department of Materials Science and Engineering, Egypt-Japan University of Science and Technology, Alexandria, Egypt mohsen.khozami@ejust.edu.eg

⁴Ahmed M.R. FathElbab is with the Department of Mechatronics and Robotics Engineering, Egypt-Japan University of Science and Technology, Alexandria, Egypt ahmed.rashad@ejust.edu.eg

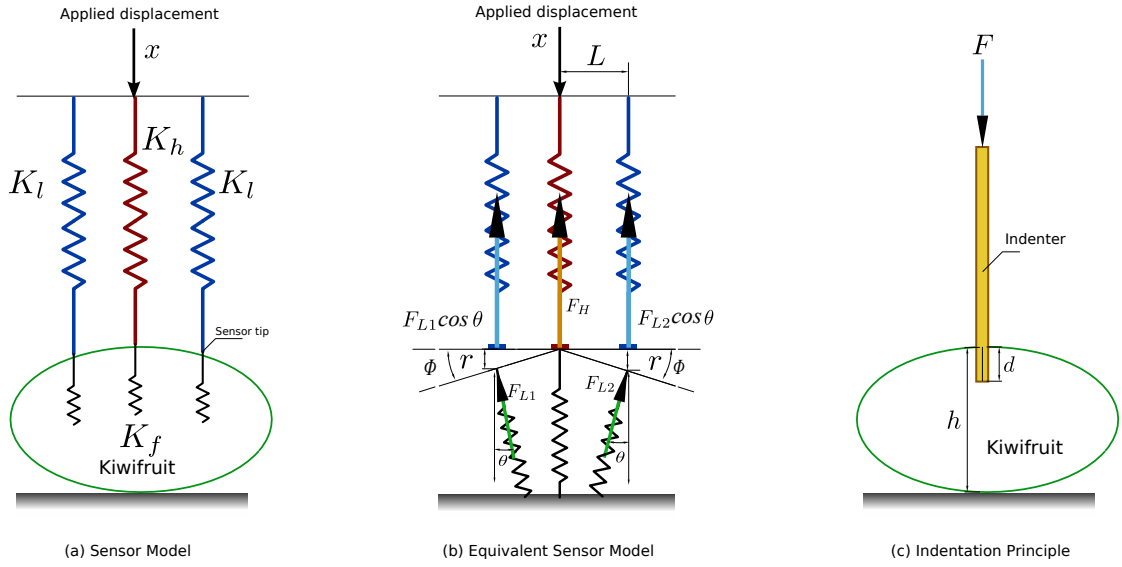


Fig. 1. The sensor model and the basic idea of the indentation principle.

ration was unstable, fluctuating, and infinite at an inclination angle of 6° during the experimentation of the sensor. An error rate of 14% was recorded in the sensor's output, which is large enough to give inaccurate results during stiffness detection applications, which could cost lives in medical applications and economic losses, especially when considering fruits marketing.

In order to tackle the above-mentioned challenges, we propose the design principles and experimental results of a three-tip tactile sensor for estimating the stiffness of fruits, using kiwifruit as a case study. Basically, our contributions are as follows; we propose:

- a design configuration based on a cantilever arrangement with piezoresistive elements, enabling the stable acquisition of sensor readings over independent trials,
- the stiffness estimation scheme based on the compact feed-forward neural networks (NN) allowing us to find effective and high-performing nonlinear relationships between instantaneous sensor readings and the ground truth of stiffness of fruits, irrespective of the measurement trial and location,
- the experiments using several kiwifruit specimens and the study of 25 feed-forward NN, converging to MSE loss at 10^{-5} across training-validation-testing in most of the cases, and clarifying the utmost predictive performance of a pyramidal class of feed-forward architectures.

II. SENSOR STRUCTURE

A. Basic Idea

We propose a tactile sensor based on a cantilever model, whose configuration considers three linear springs with stiffness K_h and K_l as shown in Fig. 1-(a). As the sensor receives the displacement x to contact the fruit, spring forces are generated in both the high and low stiffness springs, as shown in Fig. 1-(b). Since both K_h and K_l are in series with the stiffness constant of the fruit K_f , the equivalent stiffness is

$$K_H = \frac{K_h K_f}{K_h + K_f}, \quad (1)$$

$$K_L = \frac{K_l K_f}{K_l + K_f}. \quad (2)$$

When an inclination angle Φ between the sensor tips and the surface of the specimen occurs, we consider the case where the inclination angles at the two low stiffness springs are equal and perpendicular to the fruit surface as shown in Fig. 1-(b). Thus the sensor output S can be expressed with respect to the reaction force component θ , as follows:

$$S = \frac{F_H}{F_{L1} \cos \theta + F_{L2} \cos \theta} \quad (3)$$

$$F_{L1} = F_{L2} = F_L = K_L(x - L \tan \Phi) \quad (4)$$

$$F_H = x K_H \quad (5)$$

where the output S is a dimensionless parameter, and L is the distance between the sensor tips. For Φ and L small, $L \tan \Phi$ becomes comparatively smaller, and can be neglected:

$$S = \frac{F_H}{2F_L \cos \theta} = \frac{K_H}{2K_L \cos \theta} = \frac{K_h(K_l + K_f)}{2K_l(K_h + K_f) \cos \theta} \quad (6)$$

Since $\cos \theta$ gives an approximate value of 1 for $0 \leq \theta < 6^\circ$, we can approximate (6) and rewrite it as follows

$$K_f = \frac{K_h K_l (1 - 2S)}{2S K_l - K_h}. \quad (7)$$

We can also use the indentation principle as shown by Fig. 1-(c) to estimate the stiffness of the fruit specimen [17]:

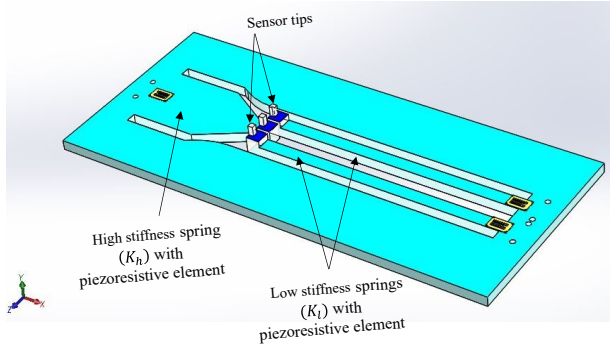


Fig. 2. The sensor model and configuration.

$$K_f = \frac{2r_i E_f C_k}{1 - \nu^2}, \quad (8)$$

where K_f , ν , F , r_i , d , h , E_f , and C_k denote the fruit stiffness, Poisson's ratio, applied force, indenter radius, indentation depth, radial height of the fruit, elastic modulus of the fruit, and the scaling factor, respectively. Here, we assume the fruit specimens to be isotropic and linearly elastic especially when indented slightly with an indenter of small area. The Poisson's ratio is set to 0.3 [18], and $C_k = 1$ is derived from a finite element analysis [19]. The indenter was assumed as a cuboid with side length of 1 mm.

III. EXPERIMENTS

A. Sensor design

Fig. 2 shows the geometry and the structure of the tactile sensor, which is realized as a cantilever beam with three-tips, each of which represents the high and the two low stiffness springs. Each spring of the sensor was fit with piezoresistive elements set at nominal resistance of 350 Ω . The stiffness of each beam can be estimated as follows:

$$K = \frac{EWt^3}{4\ell^3}, \quad (9)$$

where K , E , I , ℓ , W , and t denote the beam stiffness, elastic modulus of the beam material, area moment of inertia about the centroidal axis of the beam, length of the beam, width of the beam, and thickness of the beam, respectively. The material of the sensor prototype was acrylic Perspex whose elastic modulus $E_h = E_l = 3 \times 10^9 \text{ N/m}^2$.

Also, we computed other dimensions that met the stiffness values of the springs as $t_h = t_l = 3$ mm, $\ell_h = 4$ cm, $\ell_l = 7.8$ cm, $W_h = 2.2$ cm, and $W_l = 0.41$ cm, in which subscripts h and l denote the corresponding high and low stiffness values as in (9). The geometry of the sensor tips are set as a cuboid of 1 mm \times 1 mm \times 3 mm. The fine tuning and study of the optimal design parameters is out of the scope of this paper.

B. Setup

We used an interface setup as shown in Fig. 3 comprising a Data Acquisition System (DAQ), Wheatstone bridge circuit (a quarter bridge and a half bridge using resistors with nominal

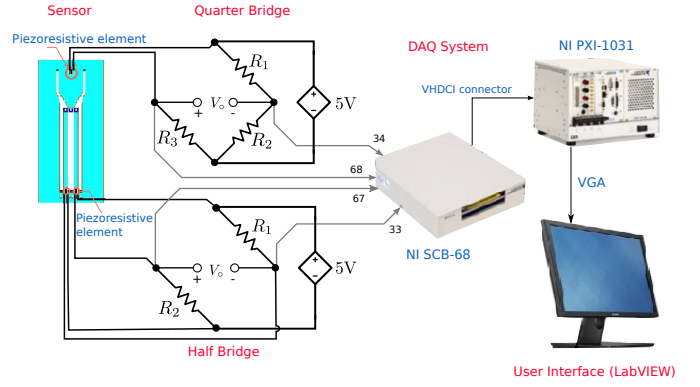


Fig. 3. The circuit interface to the sensor.

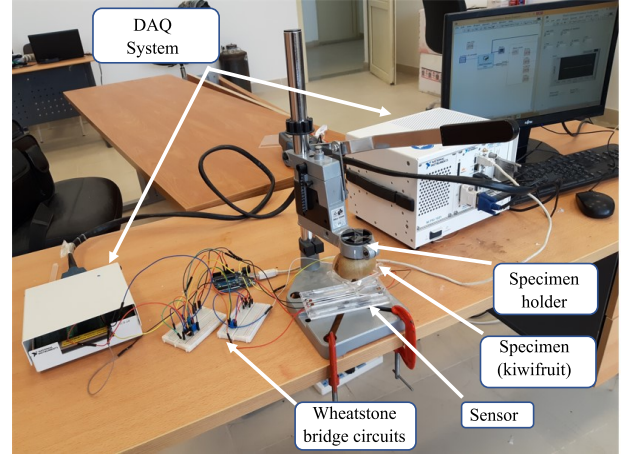


Fig. 4. Experiment setup.

resistance of 330 Ω), a LabVIEW-based user interface. Fig. 4 shows the key components in our experiment setup. The fruit specimen is fixed with a specimen holder which has a displacement gauge. When the specimen is displaced vertically downward, contact with the fixed sensor occurs, causing variation in resistance that is proportional to the induced strain. The Wheatstone bridge captures the resistance change and renders voltage signals to the DAQ (NI SCB-68 and NI PXI-1031). Then, the output voltages are converted to equivalent forces using the calibration factors of the low and high stiffness springs. For calibration, we used loads attached to the end of the sensor tips. The computed forces were mapped to sensor outputs by (6).

To study the performance of the sensor, we used six kiwifruit samples with diverse ripeness levels and elastic moduli, and to obtain readings from the sensor output:

- A displacement against the sensor tips at a maximum distance of 5 mm was conducted.
- We repeated the above four consecutive times, and by applying displacement at different points on the surface of the fruits.

Fig. 5-(a) and Fig. 5-(b) show the results of the calibration of the sensor tips over four independent trials. By observing the

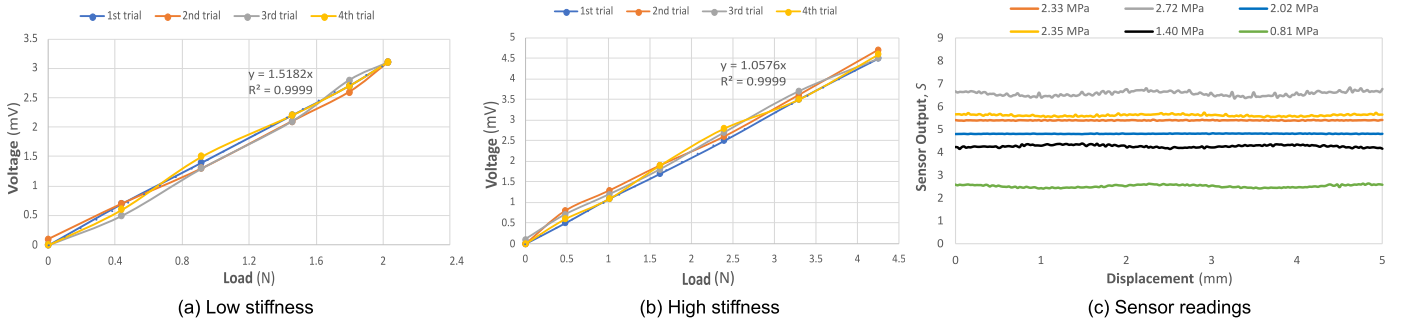


Fig. 5. (a, b) Calibration of the sensor and (c) experimental sensor output for kiwifruits of various elastic modulus E_f .

profiles of Fig. 5-(a) and Fig. 5-(b), we can note the relationship between voltage and load. For simplicity and without loss of generality, we used the average over four independent trials to map between voltages derived from the sensor's output to their corresponding load metric.

In order to show the performance of the sensor, Fig. 5-(c) shows the sensor output as a function of the applied displacement. By observing Fig. 5-(c), we note the following:

- The sensor readings remain relatively stable across the displacement range with little fluctuations.
- The sensor readings of different kiwifruits remain different, and small (large) values of sensor readings are associated to small (large) values of the elastic modulus of the kiwifruits.

The above-mentioned imply the possibility to find relationships between the sensor readings and their corresponding true stiffness/elastic modulus.

C. Stiffness approximation

We can estimate the stiffness of the fruit based on the nonlinear relationship:

$$f : S \rightarrow K_f, \quad (10)$$

where f denotes the function approximation scheme, S is the instantaneous sensor readings, and the K_f is the corresponding true stiffness of the fruit associated to the true elastic modulus E_f . Since the above represents a nonlinear regression problem, we studied the performance of Neural Networks (NN) as a universal function approximation scheme. In the above,

- S can be obtained from the instantaneous sensor readings. However, it is important to note that the K_f obtained from (7) relates directly with the instantaneous sensor output S and hence, it is affected by the nonlinearity of the sensor;
- K_f can be obtained from E_f as depicted by (8), and following the key indentation concept of Fig. 1-(c) to estimate the ground truth of the stiffness of kiwifruit samples. As such, from compression tests we found the stiffness of kiwifruit samples to be at 2.33 MPa, 2.72 MPa, 2.02 MPa, 2.35 MPa, 1.40 MPa, and at 0.81 MPa.

In line with the above notion, we evaluated the feedforward neural networks with varying number of parameters and diverse

TABLE I OVERVIEW OF THE ARCHITECTURE OF NEURAL NETWORK MODELS

Model	Hidden layers	Model	Hidden layers
NN1	[5 10]	NN14	[30 20 10]
NN2	[10 5]	NN15	[20 20 20]
NN3	[5 5 5]	NN16	[10 40 10]
NN4	[15]	NN17	[15 25 35]
NN5	[10 20]	NN18	[35 25 15]
NN6	[20 10]	NN19	[25 25 25]
NN7	[10 10 10]	NN20	[15 45 15]
NN8	[30]	NN21	[20 30 40]
NN9	[5 15 25]	NN22	[40 30 20]
NN10	[25 15 5]	NN23	[30 30 30]
NN11	[15 15 15]	NN24	[20 50 20]
NN12	[5 35 5]	NN25	[25 25 25 25]
NN13	[10 20 30]		

set of architecture of hidden layers, as shown by Table I. As such, we considered 25 networks with up to 100 nodes in which the layers were organized in a pyramidal, planar and ascending distribution. Our key motivation in considering a small number of parameters is to achieve the space-efficient and fast learning schemes, which is advantageous when deploying in small-scale embedded systems and resource-constrained computing environments.

For learning and evaluation, we proceeded as follows:

- Training data used in our experiments consisted of the union of the instantaneous sensor readings over four independent trials, each of which was retrieved at different positions in the fruit. Naturally, the sensor readings at different locations in the fruit are different among each other.
- For learning scheme, we used the Levenberg–Marquardt algorithm with loss function set as the Mean Squared Error (MSE); and for termination criterion, we used 5000 epochs with 1000 as the maximum number of validation checks before training stopped.
- To evaluate the performance over independent scenarios, we trained all the NN architectures over 10 independent runs using subsets derived from the ten-fold split scheme, yielding $250 = 25 \text{ networks} \times 10 \text{ independent runs}$ learning scenarios.

To portray the learning performance of the neural network schemes, Fig. 6 shows the convergence of the loss function over the training, validation and testing phases of 250 learning

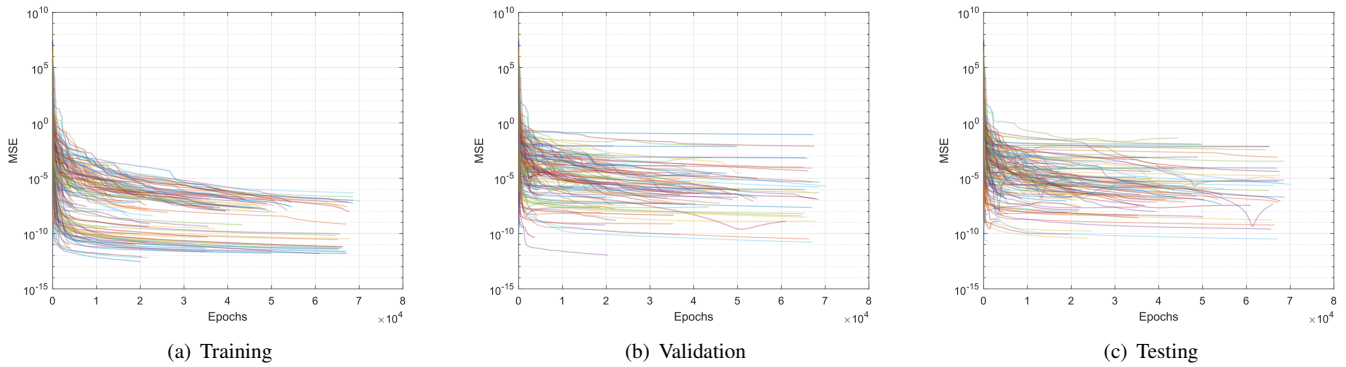


Fig. 6. Convergence of the loss function of Neural Network models using the training data. In each figure, the x-axis shows the number of epochs, and the y-axis is the MSE over ten different runs (in log-scale).

	NN1	NN2	NN3	NN4	NN5	NN6	NN7	NN8	NN9	NN10	NN11	NN12	NN13	NN14	NN15	NN16	NN17	NN18	NN19	NN20	NN21	NN22	NN23	NN24	NN25	
NN1		[+]	[+]	[+]	[+]	[+]	[+]	[+]	[+]	[+]	[+]	[+]	[+]	[+]	[+]	[+]	[+]	[+]	[+]	[+]	[+]	[+]	[+]	[+]	[+]	
NN2	[+]		[+]	[+]	[+]	[+]	[+]	[+]	[+]	[+]	[+]	[+]	[+]	[+]	[+]	[+]	[+]	[+]	[+]	[+]	[+]	[+]	[+]	[+]	[+]	[+]
NN3	[+]	[+]		[+]	[+]	[+]	[+]	[+]	[+]	[+]	[+]	[+]	[+]	[+]	[+]	[+]	[+]	[+]	[+]	[+]	[+]	[+]	[+]	[+]	[+]	[+]
NN4	[+]	[+]	[+]		[+]	[+]	[+]	[+]	[+]	[+]	[+]	[+]	[+]	[+]	[+]	[+]	[+]	[+]	[+]	[+]	[+]	[+]	[+]	[+]	[+]	[+]
NN5	[+]	[+]	[+]	[+]		[+]	[+]	[+]	[+]	[+]	[+]	[+]	[+]	[+]	[+]	[+]	[+]	[+]	[+]	[+]	[+]	[+]	[+]	[+]	[+]	[+]
NN6	[+]	[+]	[+]	[+]	[+]		[+]	[+]	[+]	[+]	[+]	[+]	[+]	[+]	[+]	[+]	[+]	[+]	[+]	[+]	[+]	[+]	[+]	[+]	[+]	[+]
NN7	[+]	[+]	[+]	[+]	[+]	[+]		[+]	[+]	[+]	[+]	[+]	[+]	[+]	[+]	[+]	[+]	[+]	[+]	[+]	[+]	[+]	[+]	[+]	[+]	[+]
NN8	[+]	[+]	[+]	[+]	[+]	[+]	[+]		[+]	[+]	[+]	[+]	[+]	[+]	[+]	[+]	[+]	[+]	[+]	[+]	[+]	[+]	[+]	[+]	[+]	[+]
NN9	[+]	[+]	[+]	[+]	[+]	[+]	[+]	[+]		[+]	[+]	[+]	[+]	[+]	[+]	[+]	[+]	[+]	[+]	[+]	[+]	[+]	[+]	[+]	[+]	[+]
NN10	[+]	[+]	[+]	[+]	[+]	[+]	[+]	[+]	[+]		[+]	[+]	[+]	[+]	[+]	[+]	[+]	[+]	[+]	[+]	[+]	[+]	[+]	[+]	[+]	[+]
NN11	[+]	[+]	[+]	[+]	[+]	[+]	[+]	[+]	[+]	[+]		[+]	[+]	[+]	[+]	[+]	[+]	[+]	[+]	[+]	[+]	[+]	[+]	[+]	[+]	[+]
NN12	[+]	[+]	[+]	[+]	[+]	[+]	[+]	[+]	[+]	[+]	[+]		[+]	[+]	[+]	[+]	[+]	[+]	[+]	[+]	[+]	[+]	[+]	[+]	[+]	[+]
NN13	[+]	[+]	[+]	[+]	[+]	[+]	[+]	[+]	[+]	[+]	[+]	[+]		[+]	[+]	[+]	[+]	[+]	[+]	[+]	[+]	[+]	[+]	[+]	[+]	[+]
NN14	[+]	[+]	[+]	[+]	[+]	[+]	[+]	[+]	[+]	[+]	[+]	[+]	[+]		[+]	[+]	[+]	[+]	[+]	[+]	[+]	[+]	[+]	[+]	[+]	[+]
NN15	[+]	[+]	[+]	[+]	[+]	[+]	[+]	[+]	[+]	[+]	[+]	[+]	[+]	[+]		[+]	[+]	[+]	[+]	[+]	[+]	[+]	[+]	[+]	[+]	[+]
NN16	[+]	[+]	[+]	[+]	[+]	[+]	[+]	[+]	[+]	[+]	[+]	[+]	[+]	[+]	[+]		[+]	[+]	[+]	[+]	[+]	[+]	[+]	[+]	[+]	[+]
NN17	[+]	[+]	[+]	[+]	[+]	[+]	[+]	[+]	[+]	[+]	[+]	[+]	[+]	[+]	[+]	[+]		[+]	[+]	[+]	[+]	[+]	[+]	[+]	[+]	[+]
NN18	[+]	[+]	[+]	[+]	[+]	[+]	[+]	[+]	[+]	[+]	[+]	[+]	[+]	[+]	[+]	[+]	[+]		[+]	[+]	[+]	[+]	[+]	[+]	[+]	[+]
NN19	[+]	[+]	[+]	[+]	[+]	[+]	[+]	[+]	[+]	[+]	[+]	[+]	[+]	[+]	[+]	[+]	[+]	[+]		[+]	[+]	[+]	[+]	[+]	[+]	[+]
NN20	[+]	[+]	[+]	[+]	[+]	[+]	[+]	[+]	[+]	[+]	[+]	[+]	[+]	[+]	[+]	[+]	[+]	[+]	[+]		[+]	[+]	[+]	[+]	[+]	[+]
NN21	[+]	[+]	[+]	[+]	[+]	[+]	[+]	[+]	[+]	[+]	[+]	[+]	[+]	[+]	[+]	[+]	[+]	[+]	[+]	[+]		[+]	[+]	[+]	[+]	[+]
NN22	[+]	[+]	[+]	[+]	[+]	[+]	[+]	[+]	[+]	[+]	[+]	[+]	[+]	[+]	[+]	[+]	[+]	[+]	[+]	[+]	[+]		[+]	[+]	[+]	[+]
NN23	[+]	[+]	[+]	[+]	[+]	[+]	[+]	[+]	[+]	[+]	[+]	[+]	[+]	[+]	[+]	[+]	[+]	[+]	[+]	[+]	[+]	[+]		[+]	[+]	[+]
NN24	[+]	[+]	[+]	[+]	[+]	[+]	[+]	[+]	[+]	[+]	[+]	[+]	[+]	[+]	[+]	[+]	[+]	[+]	[+]	[+]	[+]	[+]	[+]		[+]	[+]
NN25	[+]	[+]	[+]	[+]	[+]	[+]	[+]	[+]	[+]	[+]	[+]	[+]	[+]	[+]	[+]	[+]	[+]	[+]	[+]	[+]	[+]	[+]	[+]	[+]	[+]	

Fig. 7. Statistical pairwise comparison of the performance of Neural Networks by the Wilcoxon test at 5% significance.

scenarios. From Fig. 6, we can note the following:

- All neural networks were able to achieve the competitive learning performances at MSE less than 1.
- It is possible to obtain MSE of 10^{-5} with about 4×10^4 epochs across the training-validation-testing phases.
- The convergence performance to the basins of the loss functions can be obtained at 4×10^4 epochs.
- Most neural networks have a tendency to decrease its loss across the testing phase, implying the feasibility to minimize the loss out of sample data.

In order to portray the performance comparison across the 25 neural net schemes, Fig. 7 shows the pairwise statistical comparisons based on the best training performance and the Wilcoxon tests with 5% significance. In Fig. 7, a sign [+]

is significantly better than a neural network in the column. Conversely, a sign [-] implies that a neural network scheme in the row of the matrix is significantly worse compared to a neural network in the column. The sign (=) implies there is no statistical difference between the performances of the neural network schemes in the row and the column. Furthermore, numbers in the matrix cells show the computed p-value from the Wilcoxon test. By observing Fig. 7, we can note the following facts:

- NN1 tends to underperform with respect to other neural network schemes.
- Neural network schemes with larger number of parameters, e.g. NN14 - NN25, tend to outperform or perform similarly compared to other architectures with few number of parameters.

- It is possible to find architectures with one layer such as NN4([15]) and NN8([30]) outperforming (or performing similarly to) 87% of other related architectures.
- It is possible to find architectures with less than 45 nodes outperforming (or performing similarly to) about 83% of other architectures. Examples are NN2 ([10 5]), NN6 ([20 10]), NN10 ([25 15 5]) which outperform about 21 neural models. By observing the arrangement of nodes, one can see that these architectures show a pyramidal organization of nodes, implying that a comparatively larger number of nodes in the first layers are key to allow low-level features to be aggregated and composed more meaningfully across the hierarchy.
- It is possible to find neural architectures outperforming (or performing similarly to) 100 % of their counterparts such as NN14([30 20 10]), NN18([35 25 15]), NN22([40 30 20]) and NN23([30 30 30]), all of which have more than 60 nodes. From the above-mentioned architectures, NN14, NN18, NN22 have a pyramidal arrangement of nodes, being in line with the above-mentioned observations showing that these organization of nodes is key to allow the meaningful aggregation of low-level features across the hierarchy.

The above observations portray the performance frontiers of configurations of feedforward neural networks with small number of parameters. Also, our observations distinguish the pyramidal class of feed-forward neural architectures offering the utmost performance for our problem. Investigating the performance of deeper architectures and the performance of symbolic regression frameworks over a large number of kiwifruit samples is in our agenda.

IV. CONCLUSION

In this paper we have proposed the design principles and experimental results of a three-tip tactile sensor for the estimation of the stiffness of fruits, using kiwifruit as a case study. Our experiments using several fruit specimens with a diverse set of ripeness show (1) the feasibility of obtaining relatively stable sensor readings over independent trials, (2) the competitive performance frontiers of stiffness approximation using 25 compact feedforward neural networks, converging to MSE at 10^{-5} in most of the cases, and (3) the effectiveness of a pyramidal class of feed-forward neural architectures offering the utmost performance. Hence, the results obtained from our neural networks have proven to solve the nonlinearity problem of our instantaneous sensor output S , thereby yielding accurate predictions of the true stiffness of the fruit. The consideration of symbolic regression frameworks to elucidate the nonlinear relationships between sensor readings and stiffness, and investigating the performance of deeper architectures over a large number of kiwifruit samples is in our future agenda.

ACKNOWLEDGMENT

The authors would like to thank the Japan International Cooperation Agency (JICA), and the Science and Technology Development Fund (STDF-12417) project of the Egyptian

Ministry of Scientific Research for their generous contributions towards this research.

REFERENCES

- [1] L. Kitinaja, S. Saran, S. K. Roy, and A. A. Kader, "Postharvest technology for developing countries: challenges and opportunities in research, outreach and advocacy," *Journal of the Science of Food and Agriculture*, vol. 91, no. 4, pp. 597–603, 2011.
- [2] Y. Chen, W. Cai, X. Zou, and H. Xiang, "Extrusion mechanical properties of fresh litchi," *Transactions of the Chinese Society of Agricultural Engineering*, vol. 27, no. 8, pp. 360–364, 2011.
- [3] H. Zhu, L. Yang, J. Fei, L. Zhao, and Z. Han, "Recognition of carrot appearance quality based on deep feature and support vector machine," *Computers and Electronics in Agriculture*, vol. 186, p. 106185, 2021.
- [4] H. Zhu, L. Yang, Y. Sun, and Z. Han, "Identifying carrot appearance quality by an improved dense capnet," *Journal of Food Process Engineering*, vol. 44, no. 1, p. e13586, 2021.
- [5] P. K. Sathy, N. K. Barpanda, A. K. Rath, and S. K. Behera, "Deep feature based rice leaf disease identification using support vector machine," *Computers and Electronics in Agriculture*, vol. 175, p. 105527, 2020.
- [6] E. H. Yossy, J. Pranata, T. Wijaya, H. Hermawan, and W. Budiharto, "Mango fruit sortation system using neural network and computer vision," *Procedia Computer Science*, vol. 116, pp. 596–603, 2017, discovery and innovation of computer science technology in artificial intelligence era: The 2nd International Conference on Computer Science and Computational Intelligence (ICCCSCI 2017).
- [7] Y. Dong, Y. Huang, B. Xu, B. Li, and B. Guo, "Bruise detection and classification in jujube using thermal imaging and densenet," *Journal of Food Process Engineering*, p. e13981.
- [8] A. Esmael, K. I. E. Ahmed, and A. M. R. FathEl-Bab, "Determination of damping coefficient of soft tissues using piezoelectric transducer," *Biomedical Microdevices*, vol. 23, no. 2, p. 23, Apr 2021.
- [9] R. Cecchi, M. Verotti, R. Capata, A. Dochshyanov, G. B. Broggiato, R. Crescenzi, M. Balucani, S. Natali, G. Razzano, F. Lucchese, A. Bagolini, P. Bellutti, E. Sciubba, and N. P. Belfiore, "Development of micro-grippers for tissue and cell manipulation with direct morphological comparison," *Micromachines*, vol. 6, no. 11, pp. 1710–1728, 2015.
- [10] S. Tian, J. Wang, and H. Xu, "Firmness measurement of kiwifruit using a self-designed device based on acoustic vibration technology," *Postharvest Biology and Technology*, vol. 187, p. 111851, 2022.
- [11] A. K. Sahani, D. Srivastava, M. Sivaprakasam, and J. Joseph, "A machine learning pipeline for measurement of arterial stiffness in a-mode ultrasound," *IEEE Transactions on Ultrasonics, Ferroelectrics, and Frequency Control*, vol. 69, no. 1, pp. 106–113, 2022.
- [12] F. Miao, X. Wang, L. Yin, and Y. Li, "A wearable sensor for arterial stiffness monitoring based on machine learning algorithms," *IEEE Sensors Journal*, vol. 19, no. 4, pp. 1426–1434, 2019.
- [13] M. Bednarek, P. Kicki, J. Bednarek, and K. Walas, "Gaining a sense of touch object stiffness estimation using a soft gripper and neural networks," *Electronics*, vol. 10, no. 1, 2021.
- [14] C. T. Nnodim, A. M. R. FathEl-Bab, B. W. Ikua, and D. N. Sila, "Design, simulation, and experimental testing of a tactile sensor for fruit ripeness detection," no. 5, pp. 59–73, 2021.
- [15] A. M. R. FathEl-Bab, T. Tamura, K. Sugano, T. Tsuchiya, O. Tabata, M. E. H. Eltaib, and M. M. Sallam, "Design and simulation of a tactile sensor for soft-tissue compliance detection," *IEEE Transactions on Sensors and Micromachines*, vol. 128, no. 5, pp. 186–192, 2008.
- [16] A. Fouly, A. M. FathEl-Bab, M. N. Nasr, and A. Abouelsoud, "Modeling and experimental testing of three-tip configuration tactile sensor for compensating the error due to soft tissue surface irregularities during stiffness detection," *Measurement*, vol. 98, pp. 112–122, 2017.
- [17] W. Hayes, L. Keer, G. Herrmann, and L. Mockros, "A mathematical analysis for indentation tests of articular cartilage," *Journal of Biomechanics*, vol. 5, no. 5, pp. 541–551, 1972.
- [18] Z. Zhou, in *Physical Properties of Agricultural Materials*. Beijing: China Agricultural Press, 1994.
- [19] M. Zhang, Y. Zheng, and A. F. Mak, "Estimating the effective young's modulus of soft tissues from indentation tests—nonlinear finite element analysis of effects of friction and large deformation," *Medical Engineering & Physics*, vol. 19, no. 6, pp. 512–517, 1997.